The Astrophysical Journal, 891:141 (9pp), 2020 March 10 https://doi.org/10.3847/1538-4357/ab7335

Revising Natal Kick Prescriptions in Population Synthesis Simulations

Nicola Giacobbo[1,2,3] and Michela Mapelli[1,2,3]
[1] Dipartimento di Fisica e Astronomia "G. Galilei," Università di Padova, vicolo dell'Osservatorio 3, I-35122 PD, Italy; giacobbo.nicola@gmail.com
[2] INAF, Osservatorio Astronomico di Padova, vicolo dell'Osservatorio 5, I-35122, PD, Italy
[3] INFN, Sezione di Padova, via Marzolo 8, I-35131, PD, Italy
Received 2019 August 28; revised 2020 February 2; accepted 2020 February 4; published 2020 March 13

Abstract

Natal kicks are a matter of debate and they significantly affect the merger rate density of compact objects. Here, we present a new simple formalism for natal kicks of neutron stars (NSs) and black holes (BHs). We describe the magnitude of the kick as $v_{\rm kick} \propto f_{\rm H05}\ m_{\rm ej}\ m_{\rm rem}^{-1}$, where $f_{\rm H05}$ is a normalization factor, drawn from a Maxwellian distribution with one-dimensional rms velocity $\sigma = 265$ km s^{-1}, $m_{\rm ej}$ is the mass of the supernova (SN) ejecta, and $m_{\rm rem}$ is the mass of the compact object. This formalism matches the proper motions of young Galactic pulsars and can naturally account for the differences between core-collapse SNe of single stars, electron-capture SNe and ultra-stripped SNe occurring in interacting binaries. Finally, we use our new kick formalism to estimate the local merger rate density of binary NSs ($R_{\rm BNS}$), BH–NS binaries ($R_{\rm BHNS}$), and binary BHs ($R_{\rm BBH}$), based on the cosmic star formation rate density and metallicity evolution. In our fiducial model, we find $R_{\rm BNS} \sim 600$ Gpc^{-3} yr^{-1}, $R_{\rm BHNS} \sim 10$ Gpc^{-3} yr^{-1}, and $R_{\rm BBH} \sim 50$ Gpc^{-3} yr^{-1}, fairly consistent with the numbers inferred from the LIGO–Virgo collaboration.

Unified Astronomy Thesaurus concepts: Binary stars (154); Supernovae (1668); Black holes (162); Gravitational waves (678)

1. Introduction

Compact objects are thought to obtain a spatial velocity at their birth (natal kick), as a result of asymmetric supernova (SN) explosions (e.g Janka & Mueller 1994; Burrows & Hayes 1996) or anisotropic emission of neutrinos (e.g., Woosley 1987; Bisnovatyi-Kogan 1993; Fryer & Kusenko 2006; Kusenko et al. 2008; Sagert & Schaffner-Bielich 2008; Tamborra et al. 2014). In addition, if the SN occurs in a binary star, we expect the so-called Blaauw kick to affect the orbital properties of the binary system, even if mass loss is completely symmetric (Blaauw 1961).

Most observational estimates of natal kicks come from pulsar proper motions (Lyne & Lorimer 1994; Hansen & Phinney 1997; Arzoumanian et al. 2002; Hobbs et al. 2005; Faucher-Giguère & Kaspi 2006). The kick distribution we can infer from these data is still a matter of debate. Hobbs et al. (2005) study proper motions of 233 Galactic pulsars. Restricting their analysis to the 73 pulsars younger than ∼3 Myr (whose proper motions were less affected by the environment), they fit a Maxwellian distribution to the natal kick velocity, with one-dimensional rms velocity $\sigma = 265$ km s^{-1}.

Other works suggest a bimodal velocity distribution of pulsars, with a first peak at low velocities (e.g., ∼0 km s^{-1} according to Fryer et al. 1998 or ∼90 km s^{-1} according to Arzoumanian et al. 2002) and a second peak at high velocities (∼500 km s^{-1} according to Arzoumanian et al. 2002, or even >600 km s^{-1}, Fryer et al. 1998). Based on VLBI data of 28 isolated pulsars, Verbunt et al. (2017) also indicate that a double Maxwellian distribution provides a significantly better fit to the observed velocity distribution than a single Maxwellian distribution.

Beniamini & Piran (2016) follow a different approach: they focus on binary neutron stars (BNSs) only and find a strong preference for small mass ejection ($\leqslant 0.5\ M_\odot$) and small natal kicks ($v_{\rm kick} \leqslant 30$ km s^{-1}). Similarly, from the analysis of $r-$process material in ultra-faint dwarf galaxies Beniamini et al. (2016) find further support for a prevalence of small natal kicks in BNSs.

The situation for black hole (BH) natal kicks is even more uncertain (see, e.g., Brandt et al. 1995; Nelemans et al. 1999; Mirabel et al. 2001, 2002; Mirabel & Rodrigues 2003; Gualandris et al. 2005; Fragos et al. 2009; Repetto et al. 2012, 2017; Wong et al. 2014). While recent studies (e.g., Repetto et al. 2017; O'Shaughnessy et al. 2017; Atri et al. 2019) suggest that several Galactic BHs received a relatively high natal kick (∼100 km s^{-1}), we are still far from inferring a distribution of BH kicks from observations.

From a theoretical perspective, hydrodynamical simulations of SN explosions have successfully shown that explosion asymmetries may arise from nonradial hydrodynamic instabilities in the collapsing core (Blondin & Mezzacappa 2006; Scheck et al. 2006; Foglizzo et al. 2007, 2015; Janka 2012, 2013). Hydrodynamical simulations show that large kick magnitudes can be achieved (Wongwathanarat et al. 2013), similar to the ones reported by Hobbs et al. (2005). Recently, Janka (2017), using the gravitational tug-boat mechanism in asymmetric neutrino-driven core-collapse SNe (CCSNe), derived a simple scaling between the natal kick, the energy of the explosion, and the amount of asymmetries.

State-of-the-art population-synthesis simulations build on the results of observational constraints and of hydrodynamical models of SN explosion. Most population-synthesis codes (e.g., BSE, Hurley et al. 2000, 2002; SEBA, Portegies Zwart & Verbunt 1996; STARTRACK, Belczynski et al. 2008; MOBSE, Mapelli et al. 2017; Giacobbo et al. 2018; SEVN Spera et al. 2019) implement neutron-star (NS) kicks through the Maxwellian distribution derived by Hobbs et al. (2005). Several codes (e.g., COMPAS, Vigna-Gómez et al. 2018; MOBSE, Giacobbo & Mapelli 2018, 2019, and COMBINE, Kruckow et al. 2018) assume different Maxwellian distributions, based on the SN mechanism (usually with a higher rms velocity for CCSNe and a smaller rms velocity for ECSNe and ultra-stripped SNe).

The treatment of BH kicks in population-synthesis simulations depends on whether the BH forms via fallback or via direct collapse. Lighter BHs, that are thought to form via fallback and to receive larger kicks (e.g., Janka 2013), are assigned natal kicks drawn from the same distribution as NS kicks (Hobbs et al. 2005), but corrected either for linear momentum conservation (e.g., Mapelli et al. 2013; Ziosi et al. 2014) or for the effect of fallback (Fryer et al. 2012). Finally, if massive BHs are allowed to form by direct collapse, no kick is usually assumed apart from the Blaauw mechanism (Fryer et al. 2012).

Several recent studies suggest that this approach is not sufficient to capture the complexity of natal kicks. In particular, Bray & Eldridge (2016) and Bray & Eldridge (2018) propose a new linear relation between the mass of the ejecta (to account for the effect of asymmetries), divided by the mass of the compact object (to conserve linear momentum), and the natal kick. Moreover, natal kicks from electron-capture SNe (ECSNe), which are less energetic than CCSNe, are expected to be significantly low (Dessart et al. 2006; Schwab et al. 2015; Gessner & Janka 2018; Giacobbo & Mapelli 2019). Furthermore, some stars in close binary systems are predicted to have their outer envelope removed and experience ultra-stripped SNe, i.e., SN explosions of naked helium stars that were stripped by their compact companion (Tauris et al. 2013, 2015). In this case, the natal kick might be lower, because of the low mass of the ejecta (Suwa et al. 2015; Tauris et al. 2017; Kruckow et al. 2018; Müller et al. 2018). Finally, recent population-synthesis studies (Chruslinska et al. 2018; Giacobbo & Mapelli 2018; Mapelli & Giacobbo 2018) suggest that very low kicks ($\leqslant$50 km s^{-1}) are crucial to match the high local merger rate density of BNSs inferred from LIGO–Virgo data (110–3840 Gpc^{-3} yr^{-1}, Abbott et al. 2019a).

Here, we propose a new simple prescription for natal kicks which is able to account for both large velocities in young isolated pulsars and small kicks in ultra-stripped SNe, ECSNe, and failed SNe. Building upon Bray & Eldridge (2016), we start from the idea that the effect of asymmetries scales with the mass of the ejecta ($m_{\rm ej}$). From linear momentum conservation, we include the dependence of the kick on compact-object mass ($m_{\rm rem}$). As a normalization, we take the Maxwellian distribution by Hobbs et al. (2005).

Hence, our new prescription can be written in the form $v_{\rm kick} \propto f_{\rm H05}\, m_{\rm ej}\, m_{\rm rem}^{-1}$, where $f_{\rm H05}$ is the kick extracted from a Maxwellian with one-dimensional rms $\sigma = 265$ km s^{-1}. For NSs formed from single stars, our formula is basically indistinguishable from Hobbs et al. (2005). For NSs that form in close binaries (going through ECSNe or ultra-stripped SNe), this formalism automatically produces very low kicks, consistent with Beniamini & Piran (2016) and Mapelli & Giacobbo (2018). Finally, low-mass BHs (which form through fallback) tend to have significantly larger kicks than massive BHs, formed via direct collapse.

This paper is organized as follows. In Section 2, we describe our new prescriptions for natal kicks, as implemented in MOBSE. Then, we show the effect of our new prescriptions on the distribution of natal kicks (Section 3) and we discuss their impact on the merger rate (Section 4). Finally, we summarize our results in Section 5.

2. Numerical Method

We implement the new prescriptions for natal kicks in our population synthesis code MOBSE, which is an updated and customized version of BSE (Hurley et al. 2000, 2002). Here we briefly summarize the main differences between MOBSE and BSE and we refer to previous papers for more details (Giacobbo et al. 2018; Giacobbo & Mapelli 2018).

2.1. MOBSE

Mass loss by stellar winds of massive hot stars is described in MOBSE as $\dot{M} \propto Z^{\beta}$, where $\beta = 0.85$, $2.45 - 2.4\,\Gamma_e$, and 0.05 for electron-scattering Eddington ratio $\Gamma_e \leqslant 2/3$, $2/3 < \Gamma_e \leqslant 1$, and $\Gamma_e > 1$, respectively (see Giacobbo et al. 2018 and references therein).

ECSNe are modeled as described in Giacobbo & Mapelli (2019). In particular, a star with a helium core mass at the base of the asymptotic giant branch $1.6 \leqslant M_{\rm BABG}/M_{\odot} < 2.25$ forms a partially degenerate carbon–oxygen core. If this star forms a degenerate oxygen–neon core that reaches a mass $M_{\rm ECSN} = 1.38\,M_{\odot}$, it collapses due to the electron-capture on ^{24}Mg and ^{20}Ne (see, e.g., Fryer et al. 2012).

CCSNe are described as in Fryer et al. (2012), including both the rapid and the delayed model. The SN shock is launched <250 and >500 ms after the onset of core collapse in the rapid model and in the delayed model, respectively. This leads to a substantial difference in the energy released by the CCSN. In both models, the mass of the compact object formed via a CCSN is determined by the final mass of the carbon–oxygen core $m_{\rm CO}$: if $m_{\rm CO} \geqslant 11\,M_{\odot}$ the star collapses to a BH directly (without mass loss), otherwise the details of the remnant mass depend on the mass of the proto-NS $m_{\rm proto}$ and on the amount of fallback. Specifically, in the rapid model the mass of the compact object is $m_{\rm rem} = m_{\rm proto} + m_{\rm fb}$, where $m_{\rm fb} = f_{\rm fb}\,(m_{\rm fin} - m_{\rm proto})$ is the mass accreted by fallback ($m_{\rm fin}$ is the mass of the star at the onset of core collapse and $f_{\rm fb}$ is the fallback parameter, as defined in Fryer et al. 2012).

In this work, we introduce a small but crucial difference with respect to the previous versions of MOBSE: the mass of the proto-NS in the rapid model is $m_{\rm proto} = 1.1\,M_{\odot}$, while in Fryer et al. (2012) and in the previous versions of MOBSE we adopted $m_{\rm proto} = 1.0\,M_{\odot}$. This change is fundamental to match the mass of observed NSs (Tauris et al. 2017), because with $m_{\rm proto} = 1.0\,M_{\odot}$ we drastically overestimated the fraction of NSs with mass $<1.2\,M_{\odot}$ (see, e.g., Giacobbo & Mapelli 2018).

Finally, MOBSE includes a treatment for pair instability and pulsational pair instability based on Spera & Mapelli (2017): if the He core mass is $135 \geqslant m_{\rm He}/M_{\odot} \geqslant 64$, the star undergoes a pair-instability SN and leaves no compact object; if the He core mass is $64 > m_{\rm He}/M_{\odot} \geqslant 32$, the star undergoes pulsational pair instability and the final mass of the compact object is calculated as $m_{\rm rem} = \alpha_{\rm P}\, m_{\rm no\,PPI}$, where $m_{\rm no\,PPI}$ is the mass of the compact object we would have obtained if we had not included pulsational pair instability in our analysis (just CCSN) and $\alpha_{\rm P}$ is a fitting parameter described in Mapelli et al. (2020).

Other changes with respect to BSE include the modeling of core radii (according to Hall & Tout 2014), the treatment of common envelope (CE, we assume that all Hertzsprung-gap donors merge during CE) and the maximum stellar mass (we extend the mass range up to 150 $M_{\odot}$, Mapelli 2016). Apart from the changes summarized in this section, single and binary

evolution in MOBSE is the same as described in Hurley et al. (2000) and Hurley et al. (2002).

2.2. Natal Kick Prescriptions

To develop the new kick prescriptions, we start from assuming that the Maxwellian distribution derived by Hobbs et al. (2005) is a description of NS kicks from single star evolution. This assumption is a simplification, as we neglect that the Hobbs et al. (2005) sample contains not only single pulsars but also pulsar binaries. On the other hand, the 46 young pulsars whose two-dimensional proper motions were used by Hobbs et al. (2005) to derive the Maxwellian distribution fit with $\sigma = 265\,\mathrm{km\,s^{-1}}$ are all single pulsars (see Figure 7 in Hobbs et al. 2005). Another caveat to keep in mind is that a fraction of these single pulsars might have been members of a binary system before their formation. Thus, if new results about proper motions of young single pulsars become available and suggest a significantly different fitting function, we can easily update our prescriptions to include the new fitting function.

Furthermore, we include in our prescriptions the mass of the ejecta $m_{\rm ej}$, because it is reasonable to assume that the magnitude of the kick depends on the total mass ejected during the SN explosion. Finally, to satisfy linear momentum conservation, we also include a term depending on the mass of the compact object $m_{\rm rem}$.

Hence, the new prescription we adopt for SN kicks can be expressed as

$$v_{\rm kick} = f_{\rm H05}\,\frac{m_{\rm ej}}{\langle m_{\rm ej}\rangle}\,\frac{\langle m_{\rm NS}\rangle}{m_{\rm rem}}, \quad (1)$$

where $f_{\rm H05}$ is a random number extracted from a Maxwellian distribution with one-dimensional rms $\sigma = 265\,\mathrm{km\,s^{-1}}$ (Hobbs et al. 2005), $\langle m_{\rm NS}\rangle$ is the average NS mass, and $\langle m_{\rm ej}\rangle$ is the average mass of the ejecta associated with the formation of an NS of mass $\langle m_{\rm NS}\rangle$ from single stellar evolution. In our calculations, we adopt $\langle m_{\rm NS}\rangle = 1.2\ \ M_\odot$ and $\langle m_{\rm ej}\rangle = 9\ \ M_\odot$, respectively. These values are calibrated at $Z = 0.02$, which is approximately the metallicity of the Milky Way. We compute $m_{\rm ej}$ as the difference between the final mass of the star (before the SN explosion) and the mass of the remnant (including mass loss due to neutrinos). The basic idea behind this normalization is that we want neutron stars formed from single star evolution at solar metallicity to receive a kick consistent with the proper motions of young single pulsars in the Milky Way (which we approximate as $f_{\rm H05}$). With this normalization, more massive compact objects receive smaller kicks because of linear momentum conservation. Similarly, compact objects that form from binary evolution (where $m_{\rm ej}$ is generally smaller than the average single NS case) also receive a smaller kick than NSs formed from single stars.

To check the impact of compact-object mass on the final kicks, we also run some tests with a second prescription, independent of $m_{\rm rem}$:

$$v_{\rm kick} = f_{\rm H05}\,\frac{m_{\rm ej}}{\langle m_{\rm ej}\rangle}. \quad (2)$$

These prescriptions have several advantages. First, they are simple to implement in population-synthesis codes. Second, they are quite universal: they can be used for both NSs and BHs, for both single and binary star evolution, for both ECSNe and CCSNe (including the case of ultra-stripped SNe).

Table 1
Models

ID	Natal kicks
Ej1	$\sigma = 265$ km s^{-1}, Equation (1)
Ej2	$\sigma = 265$ km s^{-1}, Equation (2)
H05	$\sigma = 265$ km s^{-1}, Equation (3)
σ15	$\sigma = 15$ km s^{-1}, Equation (3)

Note. Column 1: name of the simulation; column 2: natal-kick prescription.

2.3. Simulation Setup

We used MOBSE to simulate a large set of both single stars and binary systems. For single stars, and for the primary star in binary systems, we randomly draw the initial mass (m_1) from a Kroupa initial mass function (Kroupa 2001) $\mathfrak{F}(m_1) \propto m_1^{-2.3}$ with $m_1 \in$ [5–150] $M_\odot$. The mass of the stellar companion in binaries is derived from the mass ratio as $\mathfrak{F}(q) \propto q^{-0.1}$ with $q = m_2/m_1 \in$ [0.1–1] (following Sana et al. 2012). Finally, the eccentricity e and the orbital period P are also drawn from the distributions proposed by Sana et al. (2012): $\mathfrak{F}(e) \propto e^{-0.42}$ (with $0 \leqslant e < 1$) and $\mathfrak{F}(P) \propto (P)^{-0.55}$ (with $P = \log_{10}(P\ \mathrm{day}^{-1}) \in$ [0.15–5.5]).

We assume the rapid model for CCSNe (Fryer et al. 2012). We assume CE efficiency $\alpha = 5$ (unless otherwise stated) and we derive λ from the formulas in Claeys et al. (2014). In Appendix, we discuss the impact of different choices of α on our main results.

We have run the following four sets of simulations (see Table 1).

Ej1: natal kicks are implemented as in Equation (1);
Ej2: natal kicks are drawn from Equation (2);
H05: natal kicks are generated from a Maxwellian with $\sigma = 265\,\mathrm{km\,s^{-1}}$ for both CCSNe and ECSNe (see model EC265α5 in Giacobbo & Mapelli 2019), plus a correction for the amount of fallback following Fryer et al. (2012) (see below Equation (3));
σ15: natal kicks are drawn from a single Maxwellian with rms $= 15\,\mathrm{km\,s^{-1}}$ for both ECSNe and CCSNe (see model CC15α5 in Giacobbo & Mapelli 2018), plus a correction for the amount of fallback as in Fryer et al. (2012).

The correction for the amount of fallback in models H05 and σ15 is implemented as follows. We draw the natal kick as

$$v_{\rm kick} = (1 - f_{\rm fb})f_{\rm H05}, \quad (3)$$

where $f_{\rm H05}$ is a random number drawn from the Maxwellian distribution, while $f_{\rm fb}$ is the fallback fraction, defined as $f_{\rm fb} = m_{\rm fb}/(m_{\rm fin} - m_{\rm proto})$, where $m_{\rm fin}$ is the mass of the star at the onset of core collapse and $m_{\rm fb}$ is the mass that falls back and is accreted by the proto-NS (Fryer et al. 2012). The main difference between our new prescriptions and Equation (3) is that the latter does not depend significantly on the mass of the ejecta (in Equation (3) $v_{\rm kick} \propto m_{\rm ej}/m_{\rm fin}$, i.e., $m_{\rm fin}$ compensates for the impact of $m_{\rm ej}$).

The direction of the kicks has been computed adopting the same prescriptions as implemented in BSE and described in the appendix of Hurley et al. (2002). In particular, kicks are

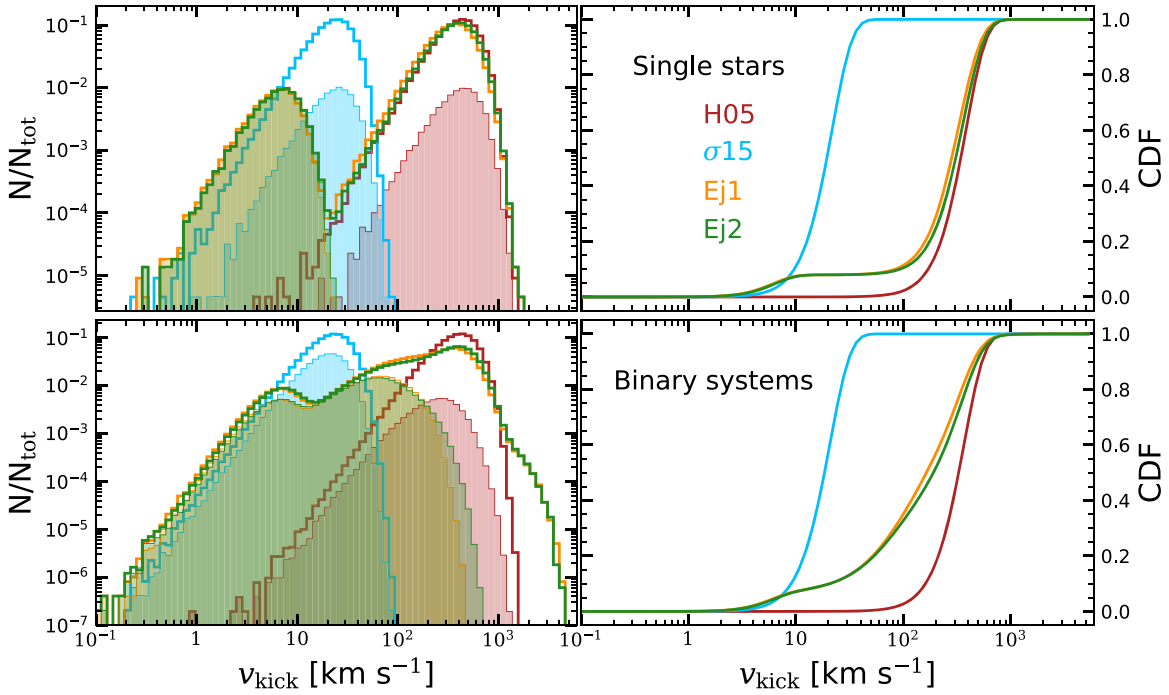

Figure 1. Left-hand panels: distribution of natal kicks for all NSs formed from single stars (top) and for those formed from binary systems (bottom) at $Z = 0.02$. Orange line: model Ej1; green: Ej2; red: H05; blue: σ15. The filled histograms represent the subset of NSs formed via ECSNe (top) and the subset of NSs that are still gravitationally bound to their companion after the SN (bottom). Right-hand panels: cumulative distribution function (CDF) of natal kicks for all NSs.

assumed to be isotropically oriented over the sphere. After randomly drawing the kick direction under this assumption, we calculate how the kick affects the orbital elements and check whether the system remains bound after the supernova explosion.

For each set of simulations we consider 12 different metallicities: $Z = 0.0002$, 0.0004, 0.0008, 0.0012, 0.0016, 0.002, 0.004, 0.006, 0.008, 0.012, 0.016, and 0.02. For each metallicity, we simulated 10^7 binary systems and 5×10^5 single stars. Thus, for each model we simulate 1.2×10^8 massive binaries and 6×10^6 single stars.

3. Results

3.1. Natal Kicks in Single Stars

The top panels of Figure 1 show the natal kick distribution of NSs born from single stars with solar metallicity ($Z = 0.02$). NS kicks from simulations Ej1 and Ej2 are extremely similar to each other. They both show two different peaks, one centered at ~400–450 km s^{-1} and produced by CCSNe, the other centered at ~6–8 km s^{-1} and produced by ECSNe. This happens because $m_{\rm ej}$ of ECSNe is significantly smaller than that of CCSNe, leading to smaller kicks. Thus, our new prescriptions are able to distinguish between CCSN kicks and ECSN kicks, without the need for a separate treatment.

The distribution of NS kicks from CCSNe in simulation H05 (drawn from a single Maxwellian with $\sigma = 265$ km s^{-1}) is remarkably similar to the peak produced by CCSNe in simulations Ej1 and Ej2. This confirms that simulations Ej1 and Ej2 are a good match to the fit by Hobbs et al. (2005) for large NS kicks. On the other hand, runs Ej1 and Ej2 can also naturally reproduce the low kicks of ECSNe. Finally, simulation σ15 produces single NS kicks that are significantly lower than the other runs, unable to explain a large fraction of the sample by Hobbs et al. (2005).

The top panels of Figure 2 show the natal kick distribution of BHs born from single stars with solar metallicity ($Z = 0.02$). All the four models predict that ~60% of BHs receive approximately no kick, because their progenitors collapse to a BH directly, without SN explosions. The remaining BHs receive a kick. Models H05 and Ej2 predict the largest maximum kicks, up to ~450 and ~550 km s^{-1}, respectively. In fact, the kick prescriptions in H05 and Ej2 do not depend on compact-object mass. Model σ15 predicts the lowest BH kicks (up to ~30 km s^{-1}), while model Ej1 ($v_{\rm kick} \leqslant 100$ km s^{-1}) is intermediate between the considered models, thanks to the dependence on $m_{\rm rem}$.

3.2. Natal Kicks in Binary Stars

The bottom panels of Figure 1 (Figure 2) shows the natal kicks of NSs (BHs) formed from the evolution of binary stars with $Z = 0.02$. Binary evolution significantly affects the distribution of NS natal kicks in all models and especially in runs Ej1 and Ej2. The Kolmogorov–Smirnov (KS) test confirms that the probability that natal kicks of NSs formed from single stars and from binary evolution are drawn from the same distribution is nearly zero ($<10^{-20}$). Table 2 shows that the median value of NS kicks is significantly lower for binary stars than for single stars in models Ej1 and Ej2. In general, binary evolution tends to increase the number of NSs with small kicks, because dissipative mass transfer tends to reduce $m_{\rm ej}$. On the other hand, binary evolution also triggers the formation of a few NSs with even larger kicks than in the case of single star evolution.

Binary evolution has a smaller impact on NS kicks in models H05 and σ15 by construction (see Table 2), because they do not depend significantly on $m_{\rm ej}$. The only effect of binary evolution on models H05 and σ15 is that mass transfer can change $m_{\rm rem}$ and the amount of fallback, hence affecting natal

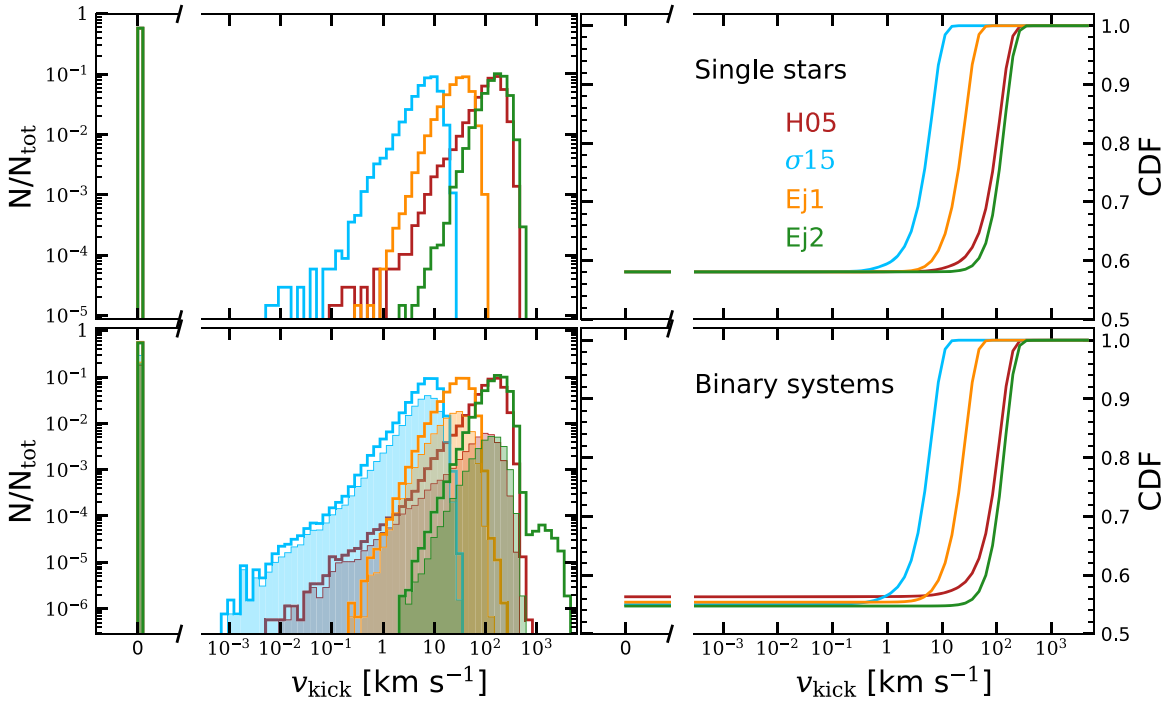

Figure 2. Same as Figure 1, but for BHs formed from single star evolution (top) and from binary star evolution (bottom) at $Z = 0.02$. The break on the x-axis allows us to show BHs with zero natal kick (formed from direct collapse).

Table 2
Median Values of Natal Kicks

Model	NS/BH	Progenitor Star	$\tilde{v}_{\rm kick}$ (km s^{-1})
Ej1	NS	single	322
Ej1	NS	binary	188
Ej2	NS	single	351
Ej2	NS	binary	218
H05	NS	single	392
H05	NS	binary	375
σ15	NS	single	22
σ15	NS	binary	21
Ej1	BH	single	30
Ej1	BH	binary	30
Ej2	BH	single	164
Ej2	BH	binary	165
H05	BH	single	127
H05	BH	binary	129
σ15	BH	single	7
σ15	BH	binary	7

Note. Column 1: model; column 2: compact-object type (NS or BH); column 3: whether the progenitor star was born as a single or a binary star; column 4: median value of natal kicks.

kicks. This affects mostly BHs, while it has a negligible impact on NSs.

The distribution of NS kicks in simulations Ej1 and Ej2 are very similar to each other, even when we account for binary evolution. As expected, NSs that remain members of a binary system after the kick (filled histograms) have significantly smaller kicks than single NSs in runs Ej1, Ej2, and H05. In model Ej1 (Ej2), the maximum kick undergone by NSs that remain in binaries is $v_{\rm kick} \sim 400$ km s^{-1} ($\sim$600 km s^{-1}), while the maximum possible NS kick is $v_{\rm kick} \sim 4500$ km s^{-1} ($\sim$4500 km s^{-1}). The maximum possible NS kick with our new models ($v_{\rm kick} \sim 4500$ km s^{-1}) is extremely unlikely, as less than $\sim 10^{-4}$% of all simulated NSs in binary systems have $v_{\rm kick} \geqslant 4000$ km s^{-1} (and less than $\sim$0.03% have $v_{\rm kick} \geqslant 2000$ km s^{-1}).

Finally, binary evolution has a different effect on BH kicks. In the case of BHs, dissipative mass transfer affects $m_{\rm rem}$, producing smaller BHs. This explains why the percentage of BHs that undergo no kick decreases (to about 5%) in all models. Table 2 shows that the median value of BH kicks is not affected by the binarity of progenitors.

3.3. Merger Efficiency

For each set of binary simulations we compute the merger efficiency, which is the number of compact-object mergers occurring in a given stellar population, integrated over the Hubble time, divided by the total initial stellar mass. As already described in Mapelli et al. (2017), the merger efficiency η is given by

$$\eta = f_{\rm bin}\, f_{\rm IMF}\, \frac{N_{\rm merg}}{M_{\rm tot,sim}}, \quad (4)$$

where $N_{\rm merg}$ is the number of mergers of binary BHs (BBHs), or BH–NS binaries (BHNSs), or binary NSs (BNSs), and $M_{\rm tot,sim}$ is the initial total mass of the simulated binary population. Since we simulated only massive binaries, we introduce two correction factors: $f_{\rm bin} = 0.5$ (to correct for the fact that $\sim$50% of stars are single, Sana et al. 2013) and $f_{\rm IMF} = 0.285$ (to account for the total mass of stars below the minimum mass we simulate).

Figure 3 shows η as a function of metallicity for all runs (see Table 1). The merger efficiency of both BBHs and BHNSs strongly depends on metallicity: BH mergers are at least two orders of magnitude more common in a metal-poor population than in a metal-rich one. This result is well known

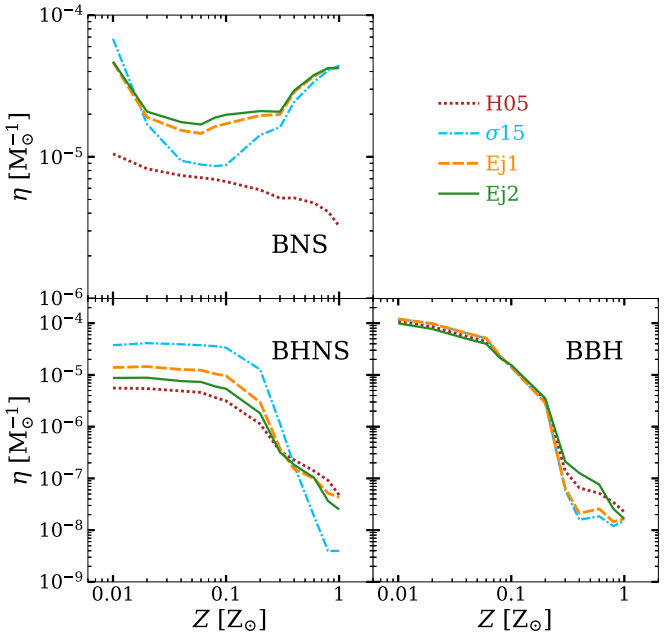

Figure 3. Merger efficiency (η from Equation (4)) as a function of the progenitor's metallicity for all sets of simulations (see Table 1). Top-left: BNSs; bottom-left: BHNSs; bottom-right: BBHs.

and is consistent with previous work (Dominik et al. 2013; Giacobbo et al. 2018; Giacobbo & Mapelli 2018; Klencki et al. 2018). The merger efficiency of BNSs depends only mildly on metallicity. The decrease of η at intermediate metallicity ($0.0004 \lesssim Z \lesssim 0.04$) in the models with relatively low kicks (Ej1, Ej2, and σ15) is caused by premature mergers of the progenitor stars, because stellar radii during the Hertzsprung gap and the red giant phase are larger at intermediate metallicity (see Giacobbo & Mapelli 2018; Spera et al. 2019). In model H05, η decreases with increasing metallicity, because the ability of CE to shrink the binary becomes decisive when SN kicks are high: at high metallicity stars lose their envelope quite effectively, reducing the impact of CE.

More importantly, Figure 3 shows that our new kick prescriptions (models Ej1, Ej2) produce approximately the same BNS merger efficiency as model σ15, which assumes unrealistically small kicks. For BHNSs, the new kick prescriptions give a merger rate efficiency more similar to H05 than to σ15. Finally, the merger efficiency of BBHs is not significantly affected by the new kick prescriptions, because most merging BBHs receive no kick (or very small kick) in all considered models.

3.4. Local Merger Rate

Following Giacobbo & Mapelli (2018) and Spera et al. (2019), we compute the local merger rate density R as

$$R = \frac{1}{H_0\, t_{\rm lb}(z=0.1)} \int_{z_{\rm max}}^{z_{\rm min}} \frac{f_{\rm loc}(z, Z)\, {\rm SFR}(z)}{(1+z)\mathcal{E}(z)} dz, \qquad (5)$$

where SFR(z) is the star formation rate density (for which we adopt the fitting formula proposed by Madau & Fragos 2017), $\mathcal{E}(z) = [\Omega_{\rm M}(1+z)^3 + \Omega_\Lambda]^{1/2}$, $t_{\rm lb}(z=0.1)$ is the look-back time at redshift $z = 0.1$, and $f_{\rm loc}(z, Z)$ is the fraction of merging systems that formed at a given redshift z and merge in the local universe ($z \leqslant 0.1$) per unit solar mass. We assume $z_{\rm max} = 15$ and $z_{\rm min} = 0$. Finally, H_0, $\Omega_{\rm M}$, and Ω_Λ are the cosmological parameters for which we take the values from Planck Collaboration et al. (2016).

The term $f_{\rm loc}(z, Z)$ clearly depends not only on redshift but also on metallicity (which is important especially for BBHs and BHNSs, see Figure 3). We derive $f_{\rm loc}(z, Z)$ directly from the merger efficiency η (Equation (4)), by assuming that all stars formed at a given redshift have the same metallicity. We describe the evolution of metallicity across cosmic time with two different models. In model *D18*, the metallicity evolves with redshift as $\log Z(z)/Z_\odot = -0.24\, z - 0.18$. This formula is the fit to the metallicity evolution of a large sample of damped Lyα absorbers (with redshift between 0 and 5) presented in De Cia et al. (2018; see their Figure 4 and Table 1). With respect to previous work (e.g., Rafelski et al. 2012, whose results we used in Giacobbo & Mapelli 2018), De Cia et al. (2018) consider a larger sample of damped Lyα absorbers and make a new correction for dust. This allows them to recover a present-day average metallicity $Z(z=0) \sim 0.66\, Z_\odot$ (where we assume $Z_\odot = 0.02$), much closer to the solar metallicity than previous work.

In the second model we adopt ($D18_{Z_\odot}$), the metallicity evolves with redshift as $\log Z(z)/Z_\odot = -0.24\, z$. This model is obtained by rescaling model *D18* to obtain $Z(z=0) = Z_\odot$. The reason for this rescaling is that metallicity measurements from galaxies in the Sloan Digital Sky Survey indicate that the average local metallicity is $Z(z=0) \sim Z_\odot$ (Gallazzi et al. 2008).

Figure 4 shows the local merger rate $R_{\rm BNS}$, $R_{\rm BHNS}$, and $R_{\rm BBH}$ for BNSs, BHNSs, and BBHs, respectively, considering both models of metallicity evolution, namely *D18* and $D18_{Z_\odot}$.

The new kick prescriptions Ej1 and Ej2 produce a BNS merger rate $R_{\rm BNS} \sim 600$ Gpc^{-3} yr^{-1}, consistent with the local merger rate inferred from GW170817 ($R_{\rm GW170817} = 110 - 3840$ Gpc^{-3} yr^{-1}, Abbott et al. 2017, 2019a). The rate from Ej1 and Ej2 is very similar to the rate we obtain with the low-kick model σ15 and about one order of magnitude higher than the rate we obtain with model H05.

All our models are consistent with the upper limit on BHNSs by Abbott et al. (2019a). Models Ej1 and Ej2 produce rates that are significantly smaller than σ15 and slightly higher than H05. Finally, the merger rate density of BBHs is extremely sensitive to metallicity. Model *D18* results in a factor of $\sim$2 higher BBH merger rate than model $D18_{Z_\odot}$, but still within the 90% credible interval inferred by the LIGO–Virgo Collaboration (LVC, $R_{\rm BBH} \sim 24$–112 Gpc^{-3} yr^{-1}, Abbott et al. 2019b). The four kick prescriptions produce approximately the same BBH merger rate density, because all of them suppress natal kicks in massive BHs by approximately the same amount.

4. Discussion

Recent studies (Chruslinska et al. 2018, 2019; Belczynski et al. 2018; Giacobbo & Mapelli 2018, 2019; Mapelli & Giacobbo 2018) have shown that it is quite difficult to match the BNS merger rate inferred from GW170817 ($R_{\rm GW170817}$) with state-of-the-art population-synthesis models. Models describing natal kicks as in Hobbs et al. (2005) produce a merger rate density lower than the range inferred from

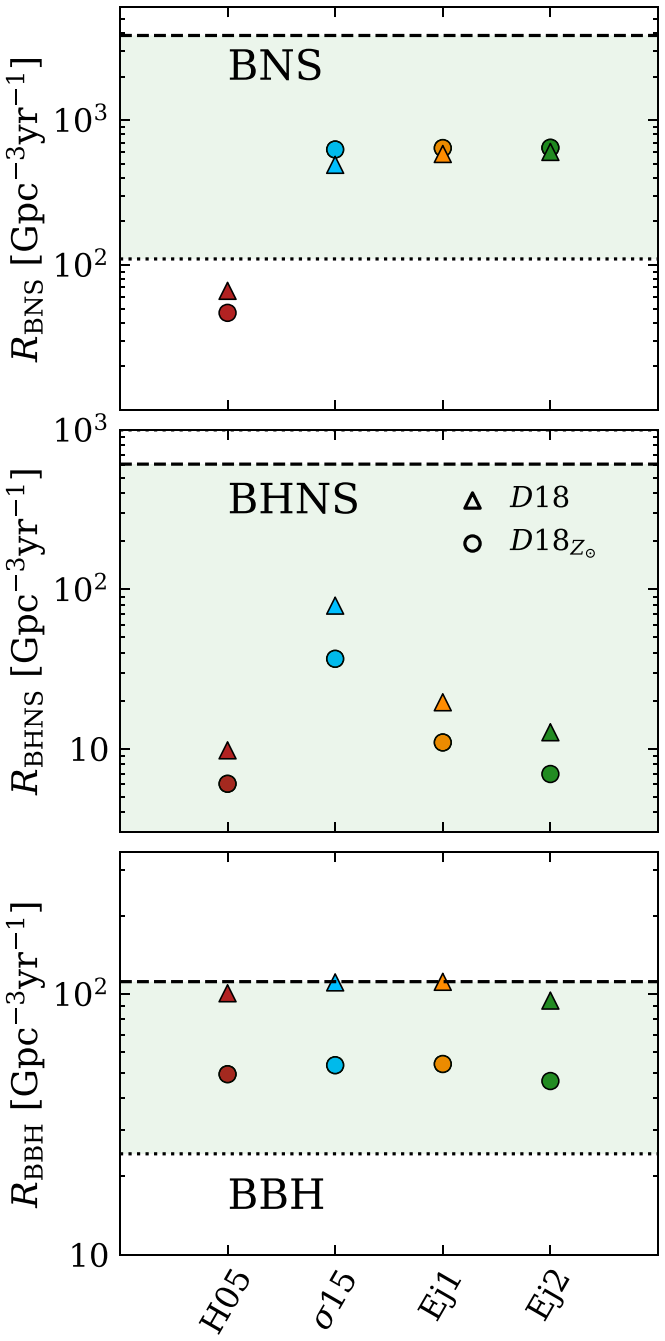

Figure 4. Local merger rate density R from Equation (5). Top, middle, and bottom panel: local merger rate density of BNSs ($R_{\rm BNS}$), BHNSs ($R_{\rm BHNS}$), and BBHs ($R_{\rm BBH}$), respectively. Triangles (circles) assume model $D18$ ($D18_{Z_\odot}$) for the cosmic evolution of metallicity. The green shaded regions represent the 90% confident interval of the merger rate density inferred by Abbott et al. (2019b) for BBHs and Abbott et al. (2019a) for BNSs and BHNSs.

GW170817. In order to match $R_{\rm GW170817}$, Giacobbo & Mapelli (2018) had to introduce model $\sigma15$ with very low natal kicks. On the other hand, model $\sigma15$ does not match the observed proper motions of young single pulsars (Hobbs et al. 2005; Verbunt et al. 2017).

Our new kick prescriptions (models Ej1 and Ej2) solve this tension with data, because they match $R_{\rm GW170817}$ and at the same time they reproduce the natal kicks of young pulsars. Moreover, Ej1 and Ej2 naturally account for the difference between kicks produced by CCSNe of single stars, ECSNe, and ultra-stripped SNe in binary stars (Tauris et al. 2017).

The only parameter we need to set to a rather unusual value in order to match $R_{\rm GW170817}$ is the α parameter of CE. Our models Ej1 and Ej2 require $\alpha \geqslant 3$ to match $R_{\rm GW170817}$ (see the Appendix) and we assume $\alpha = 5$ as a fiducial value. According to the $\alpha-$formalism (Webbink 1984, 1985; de Kool 1990), values of $\alpha > 1$ require that additional sources of energy assist the orbital energy of the system in ejecting the envelope (see Ivanova et al. 2013 for a review). Recently, Fragos et al. (2019) have presented one-dimensional hydrodynamic simulations of a neutron-star binary evolving through CE. Their results support very large values of $\alpha \approx 5$, consistent with our work. Once more, this highlights the need for a better physical model of the CE process. Another possibility is that GW170817 was a very lucky event, leading to an overestimate of the local merger rate. A more accurate estimate of the observed merger rate will be available in the next few months, because the third observing run of LVC is currently ongoing.

The key ingredient in our prescriptions is the dependence of $v_{\rm kick}$ on the mass of the ejecta ($v_{\rm kick} \propto m_{\rm ej}$). Models adopting the fallback formalism (Fryer et al. 2012) predict significantly larger kicks for NSs even if they come from ultra-stripped SNe, because in this formalism $v_{\rm kick} \propto m_{\rm ej}/m_{\rm fin}$ (i.e., the contribution of $m_{\rm ej}$ to the kick is compensated by the stellar mass $m_{\rm fin}$ at the onset of the SN). The only models that predict a similar behavior to our prescriptions are those presented in Bray & Eldridge (2016, 2018). Bray & Eldridge (2018) derive a BNS merger rate density $R_{\rm BNS} \sim 3860$ Gpc^{-3} yr^{-1}. The difference with respect to our results might arise from the calculation of the local merger rate (Bray & Eldridge 2018 consider only the local SFR, without taking into account the evolution of metallicity across cosmic time) and from different population-synthesis codes.

5. Summary

We have proposed a new simple formalism to implement NS and BH kicks in population-synthesis simulations. We describe kick velocities as $v_{\rm kick} \propto f_{\rm H05}\, m_{\rm ej}^{-1}\, m_{\rm rem}$, where $f_{\rm H05}$ is a random number drawn from a Maxwellian distribution with one-dimensional rms $\sigma = 265$ km s^{-1} (Hobbs et al. 2005), $m_{\rm ej}$ is the mass of the ejecta, and $m_{\rm rem}$ the mass of the compact object. We have included this formalism in our population-synthesis code MOBSE.

This formalism can naturally account for the differences between core-collapse SNe (CCSNe) of single stars and electron-capture SNe (ECSNe) or ultra-stripped SNe occurring in binary systems. In fact, CCSNe of single stars have larger values of $m_{\rm ej}$ than ECSNe, ultra-stripped SNe and other SNe occurring in interacting binaries. Hence, the kicks of NSs in interacting binary systems are significantly lower than the kicks of single NSs (Figure 1 and Table 2).

The kicks of BHs are generally lower than the kicks of NSs (Figure 2 and Table 2), because $m_{\rm rem}$ is significantly larger and $m_{\rm ej}$ is generally lower than for NSs (in the case of direct collapse $m_{\rm ej} = 0$, thus the kick is zero).

We estimate the local merger rate density of BNSs ($R_{\rm BNS}$), BHNSs ($R_{\rm BHNS}$), and BBHs ($R_{\rm BBH}$) with the new kick formalism. The merger rate density of BBHs and BHNSs is extremely sensitive to metallicity evolution. With the new kick prescription Ej1 (Ej2), we find $R_{\rm BBH} \sim 53$ Gpc^{-3} yr^{-1}

($\sim$46 Gpc^{-3} yr^{-1}) and $\mathcal{R}_{\rm BHNS} \sim 10$ Gpc^{-3} yr^{-1} ($\sim$7 Gpc^{-3} yr^{-1}), when adopting model $D18_{Z_\odot}$ for the cosmic evolution of metallicity. These results are consistent with estimates from the LVC (Abbott et al. 2019a, 2019b).

The BNS merger rate density depends very mildly on metallicity evolution. With the new kick formalism we estimate $\mathcal{R}_{\rm BNS} \sim 640$ Gpc^{-3} yr^{-1} (adopting model $D18_{Z_\odot}$ for the cosmic evolution of metallicity), consistent with the rate inferred from GW170817 (Abbott et al. 2019a). Interestingly, the BNS merger rate density we find with the new kick prescriptions is extremely close to the one we derived with our previous model $\sigma15$ (Giacobbo & Mapelli 2018), that assumes extremely low NS kicks (drawn from a Maxwellian with one-dimensional rms $\sigma = 15$ km s^{-1}). Model $\sigma15$ matches $\mathcal{R}_{\rm GW170817}$ but is in tension with the proper motions of several young Galactic pulsars, while the new kick formalism overcomes this issue.

In conclusion, our new kick formalism is consistent with both observations of proper motions from young Galactic pulsars (Hobbs et al. 2005) and with the merger rate density of BBHs, BHNSs, and BNSs inferred from the LVC (Abbott et al. 2019a, 2019b). These results, together with its intrinsic simplicity, make our new kick formalism an interesting prescription for population synthesis simulations.

We thank the anonymous referee for their useful suggestions. We also thank Mario Spera, Alessandro Ballone, Mario Pasquato, and Filippo Santoliquido for fruitful discussions. We acknowledge financial support by the European Research Council for the ERC Consolidator grant DEMOBLACK, under contract No. 770017. This work benefited from support by the International Space Science Institute (ISSI), Bern, Switzerland, through its International Team programme ref. No. 393 The Evolution of Rich Stellar Populations and BH Binaries (2017–18).

Software: MOBSE (Giacobbo et al. 2018), astropy (Astropy Collaboration et al. 2013), filltex (Gerosa & Vallisneri 2017).

Appendix
Effects of CE Efficiency on the Local Merger Rate Density

In the main text we have assumed a fixed value for the efficiency of CE ($\alpha = 5$). In this section, we discuss the impact of α on the merger rate density. To this purpose, we have run eight additional models varying the CE efficiency: Ej1α1, Ej1α2, Ej1α3, and Ej1α4 are the same as Ej1, but for $\alpha = 1$–4, respectively. Similarly, Ej2α1, Ej2α2, Ej2α3, and Ej2α4 are the same as Ej2, but for $\alpha = 1$–4, respectively. For each model, we have run the same set of simulations as for the ones reported in Table 1. We find that the merger rate density of BNSs strongly correlates with the value of α (see Figure 5). Only values of α significantly larger than 2 are consistent with the BNS merger rate density inferred from the LVC. The merger rate density of BHNSs shows basically the opposite trend, with the larger value of $\mathcal{R}_{\rm BHNS}$ being achieved for the smaller values of α. Finally, the merger rate density of BBHs seems to indicate a bell-shaped dependence on α, with the larger values of $\mathcal{R}_{\rm BBH}$ obtained for $\alpha \sim 2$–3. In a follow-up paper, we will discuss the physical motivations of this behavior.

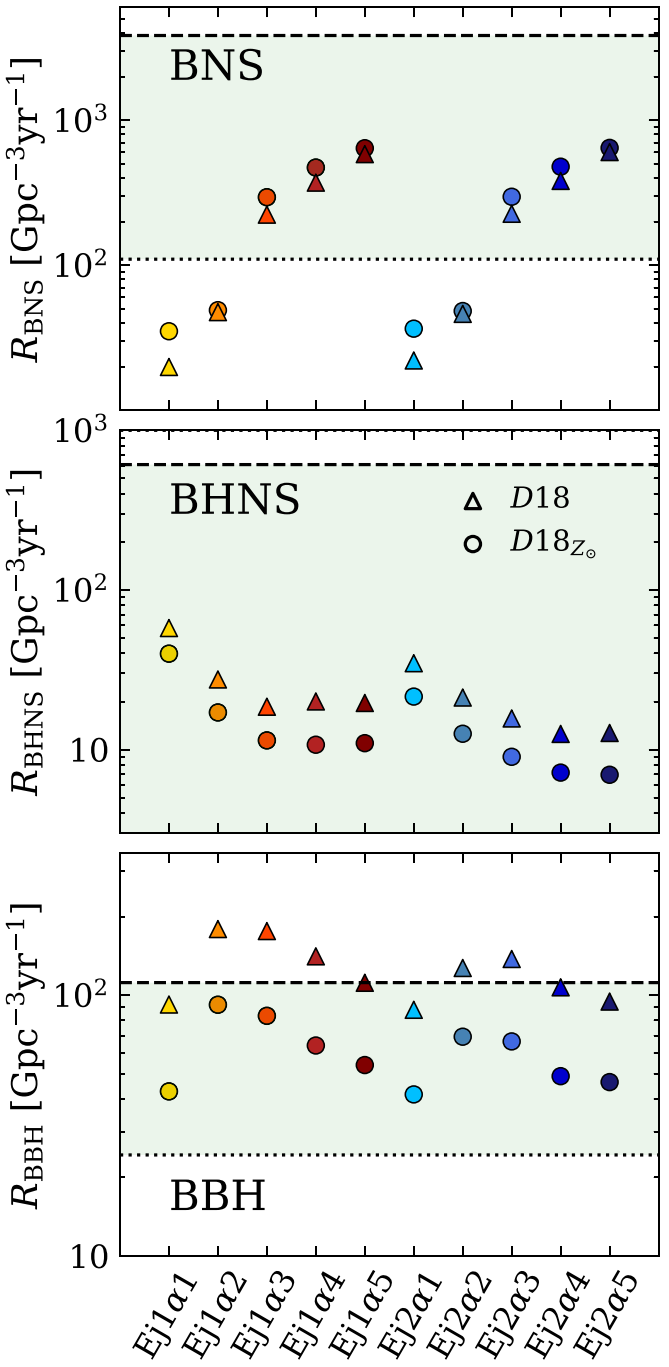

Figure 5. Local merger rate density $\mathcal{R}$ from Equation (5). Same as Figure 4, but here we consider only models Ej1 and Ej2 and we investigate the effect of different values of CE efficiency $\alpha = 1$–5 (corresponding to models Ej1α1/Ej2α1, Ej1α2/Ej2α2, Ej1α3/Ej2α3, Ej1α4/Ej2α4, and Ej1α5/Ej2α5). Models labeled as Ej1α5 and Ej2α5 are the same as our models Ej1 and Ej2 in the rest of the paper (hence $\alpha = 5$).

ORCID iDs

Nicola Giacobbo https://orcid.org/0000-0002-8339-0889
Michela Mapelli https://orcid.org/0000-0001-8799-2548

References

Abbott, B. P., Abbott, R., Abbott, T. D., et al. 2017, PhRvL, 119, 161101
Abbott, B. P., Abbott, R., Abbott, T. D., et al. 2019a, PhRvX, 9, 031040
Abbott, B. P., Abbott, R., Abbott, T. D., et al. 2019b, ApJL, 882, L24

Arzoumanian, Z., Chernoff, D. F., & Cordes, J. M. 2002, ApJ, 568, 289
Astropy Collaboration, Robitaille, T. P., Tollerud, E. J., et al. 2013, A&A, 558, A33
Atri, P., Miller-Jones, J. C. A., Bahramian, A., et al. 2019, MNRAS, 489, 3116
Belczynski, K., Askar, A., Arca-Sedda, M., et al. 2018, A&A, 615, A91
Belczynski, K., Kalogera, V., Rasio, F. A., et al. 2008, ApJS, 174, 223
Beniamini, P., Hotokezaka, K., & Piran, T. 2016, ApJL, 829, L13
Beniamini, P., & Piran, T. 2016, MNRAS, 456, 4089
Bisnovatyi-Kogan, G. S. 1993, A&AT, 3, 287
Blaauw, A. 1961, BAN, 15, 265
Blondin, J. M., & Mezzacappa, A. 2006, BAAS, 38, 1099
Brandt, W. N., Podsiadlowski, P., & Sigurdsson, S. 1995, MNRAS, 277, L35
Bray, J. C., & Eldridge, J. J. 2016, MNRAS, 461, 3747
Bray, J. C., & Eldridge, J. J. 2018, MNRAS, 480, 5657
Burrows, A., & Hayes, J. 1996, PhRvL, 76, 352
Chruslinska, M., Belczynski, K., Klencki, J., & Benacquista, M. 2018, MNRAS, 474, 2937
Chruslinska, M., Nelemans, G., & Belczynski, K. 2019, MNRAS, 482, 5012
Claeys, J. S. W., Pols, O. R., Izzard, R. G., Vink, J., & Verbunt, F. W. M. 2014, A&A, 563, A83
De Cia, A., Ledoux, C., Petitjean, P., & Savaglio, S. 2018, A&A, 611, A76
de Kool, M. 1990, ApJ, 358, 189
Dessart, L., Burrows, A., Ott, C. D., et al. 2006, ApJ, 644, 1063
Dominik, M., Belczynski, K., Fryer, C., et al. 2013, ApJ, 779, 72
Faucher-Giguère, C.-A., & Kaspi, V. M. 2006, ApJ, 643, 332
Foglizzo, T., Galletti, P., Scheck, L., & Janka, H.-T. 2007, ApJ, 654, 1006
Foglizzo, T., Kazeroni, R., Guilet, J., et al. 2015, PASA, 32, e009
Fragos, T., Andrews, J. J., Ramirez-Ruiz, E., et al. 2019, ApJ, 883, L45
Fragos, T., Willems, B., Kalogera, V., et al. 2009, ApJ, 697, 1057
Fryer, C., Burrows, A., & Benz, W. 1998, ApJ, 496, 333
Fryer, C. L., Belczynski, K., Wiktorowicz, G., et al. 2012, ApJ, 749, 91
Fryer, C. L., & Kusenko, A. 2006, ApJS, 163, 335
Gallazzi, A., Brinchmann, J., Charlot, S., & White, S. D. M. 2008, MNRAS, 383, 1439
Gerosa, D., & Vallisneri, M. 2017, JOSS, 2, 222
Gessner, A., & Janka, H.-T. 2018, ApJ, 865, 61
Giacobbo, N., & Mapelli, M. 2018, MNRAS, 480, 2011
Giacobbo, N., & Mapelli, M. 2019, MNRAS, 482, 2234
Giacobbo, N., Mapelli, M., & Spera, M. 2018, MNRAS, 474, 2959
Gualandris, A., Colpi, M., Portegies Zwart, S., & Possenti, A. 2005, ApJ, 618, 845
Hall, P. D., & Tout, C. A. 2014, MNRAS, 444, 3209
Hansen, B. M. S., & Phinney, E. S. 1997, MNRAS, 291, 569
Hobbs, G., Lorimer, D. R., Lyne, A. G., & Kramer, M. 2005, MNRAS, 360, 974
Hurley, J. R., Pols, O. R., & Tout, C. A. 2000, MNRAS, 315, 543
Hurley, J. R., Tout, C. A., & Pols, O. R. 2002, MNRAS, 329, 897
Ivanova, N., Justham, S., Chen, X., et al. 2013, A&ARv, 21, 59
Janka, H.-T. 2012, ARNPS, 62, 407
Janka, H.-T. 2013, MNRAS, 434, 1355
Janka, H.-T. 2017, ApJ, 837, 84
Janka, H.-T., & Mueller, E. 1994, A&A, 290, 496
Klencki, J., Moe, M., Gladysz, W., et al. 2018, A&A, 619, A77
Kroupa, P. 2001, MNRAS, 322, 231
Kruckow, M. U., Tauris, T. M., Langer, N., Kramer, M., & Izzard, R. G. 2018, MNRAS, 481, 1908
Kusenko, A., Mandal, B. P., & Mukherjee, A. 2008, PhRvD, 77, 123009
Lyne, A. G., & Lorimer, D. R. 1994, Natur, 369, 127
Madau, P., & Fragos, T. 2017, ApJ, 840, 39
Mapelli, M. 2016, MNRAS, 459, 3432
Mapelli, M., & Giacobbo, N. 2018, MNRAS, 479, 4391
Mapelli, M., Giacobbo, N., Ripamonti, E., & Spera, M. 2017, MNRAS, 472, 2422
Mapelli, M., Spera, M., Montanari, E., et al. 2020, ApJ, 888, 76
Mapelli, M., Zampieri, L., Ripamonti, E., & Bressan, A. 2013, MNRAS, 429, 2298
Mirabel, I. F., Dhawan, V., Mignani, R. P., Rodrigues, I., & Guglielmetti, F. 2001, Natur, 413, 139
Mirabel, I. F., Mignani, R., Rodrigues, I., et al. 2002, A&A, 395, 595
Mirabel, I. F., & Rodrigues, I. 2003, Sci, 300, 1119
Müller, B., Gay, D. W., Heger, A., Tauris, T. M., & Sim, S. A. 2018, MNRAS, 479, 3675
Nelemans, G., Tauris, T. M., & van den Heuvel, E. P. J. 1999, A&A, 352, L87
O'Shaughnessy, R., Gerosa, D., & Wysocki, D. 2017, PhRvL, 119, 011101
Planck Collaboration, Ade, P. A. R., Aghanim, N., et al. 2016, A&A, 594, A13
Portegies Zwart, S. F., & Verbunt, F. 1996, A&A, 309, 179
Rafelski, M., Wolfe, A. M., Prochaska, J. X., Neeleman, M., & Mendez, A. J. 2012, ApJ, 755, 89
Repetto, S., Davies, M. B., & Sigurdsson, S. 2012, MNRAS, 425, 2799
Repetto, S., Igoshev, A. P., & Nelemans, G. 2017, MNRAS, 467, 298
Sagert, I., & Schaffner-Bielich, J. 2008, A&A, 489, 281
Sana, H., de Koter, A., de Mink, S. E., et al. 2013, A&A, 550, A107
Sana, H., de Mink, S. E., de Koter, A., et al. 2012, Sci, 337, 444
Scheck, L., Kifonidis, K., Janka, H.-T., & Müller, E. 2006, A&A, 457, 963
Schwab, J., Quataert, E., & Bildsten, L. 2015, MNRAS, 453, 1910
Spera, M., & Mapelli, M. 2017, MNRAS, 470, 4739
Spera, M., Mapelli, M., Giacobbo, N., et al. 2019, MNRAS, 485, 889
Suwa, Y., Yoshida, T., Shibata, M., Umeda, H., & Takahashi, K. 2015, MNRAS, 454, 3073
Tamborra, I., Hanke, F., Janka, H.-T., et al. 2014, ApJ, 792, 96
Tauris, T. M., Kramer, M., Freire, P. C. C., et al. 2017, ApJ, 846, 170
Tauris, T. M., Langer, N., Moriya, T. J., et al. 2013, ApJL, 778, L23
Tauris, T. M., Langer, N., & Podsiadlowski, P. 2015, MNRAS, 451, 2123
Verbunt, F., Igoshev, A., & Cator, E. 2017, A&A, 608, A57
Vigna-Gómez, A., Neijssel, C. J., Stevenson, S., et al. 2018, MNRAS, 481, 4009
Webbink, R. F. 1984, ApJ, 277, 355
Webbink, R. F. 1985, in Interacting Binary Stars, ed. J. E. Pringle & R. A. Wade (Cambridge: Cambridge Univ. Press), 39
Wong, T.-W., Valsecchi, F., Ansari, A., et al. 2014, ApJ, 790, 119
Wongwathanarat, A., Janka, H.-T., & Müller, E. 2013, A&A, 552, A126
Woosley, S. E. 1987, in IAU Symp. 125, The Origin and Evolution of Neutron Stars, ed. D. J. Helfand & J.-H. Huang (Dordrecht: Reidel), 255
Ziosi, B. M., Mapelli, M., Branchesi, M., & Tormen, G. 2014, MNRAS, 441, 3703